

Article

Characteristic Analysis of Compact Spectrometer Based on Off-Axis Meta-Lens

Yi Zhou, Rui Chen and Yungui Ma *

Centre for Optical and Electromagnetic Research, State Key Lab of Modern Optical Instrumentation, Zhejiang University, Hangzhou 310058, China; zhouyi2016@zju.edu.cn (Y.Z.); chen_rui@zju.edu.cn (R.C.)

* Correspondence: yungui@zju.edu.cn; Tel.: +86-571-88206514-209

Received: 18 January 2018; Accepted: 23 February 2018; Published: 26 February 2018

Abstract: Ultra-compact spectrometers with high-resolution and/or broadband features have long been pursued for their wide application prospects. The off-axis meta-lens, a new species of planar optical instruments, provides a unique and feasible way to realize these goals. Here we give a detailed investigation of the influences of structural parameters of meta-lens-based spectrometers on the effective spectral range and the spectral resolution using both wave optics and geometrical optics methods. Aimed for different usages, two types of meta-lens based spectrometers are numerically proposed: one is a wideband spectrometer working at 800–1800 nm wavelengths with the spectral resolution of 2–5 nm and the other is a narrowband one working at the 780–920 nm band but with a much higher spectral resolution of 0.15–0.6 nm. The tolerance for fabrication errors is also discussed in the end. These provides a prominent way to design and integrate planar film-based spectrometers for various instrumental applications.

Keywords: meta-lens; metasurface; spectrometer; dispersion; off-axis optical system

1. Introduction

Recent progresses on micro/nano-photonics have become a turning point for the transformation of traditional optical systems [1]. Metasurfaces, ultrathin planar structures patterned by monolithic subwavelength elements on surfaces, provide a new way to transform the incident wavefront to the desired forms by controlling the amplitude, phase and polarization of electromagnetic fields [2–6]. Compared with their traditional counterparts, metasurfaces have emerged as unparalleled devices to realize miniaturized, on-chip integrated and multifunctional optical systems [7–10]. Tremendous breakthroughs in the field of metasurface have given rise to expansive applications ranging from planar imaging lenses [8,9,11–14], holograms [15–19], spectrometers [20,21], nonlinear devices [22,23] and even to invisible cloaks [24–26], etc.

Spectroscopy, a fundamental scientific instrument which has developed for hundreds of years since Newton elaborated his discover that the sunlight is made up of a mixture of colors in 1672 [27], is of significant importance to physics [28–30], astronomy [31–33] and chemistry [34–36]. As pivotal components in spectroscopy, traditional spectrometers usually employ isolated dispersive elements (mostly gratings or prisms) and focusing lenses, which makes the whole system bulky, complicated and unsuitable for integration [21]. To produce miniature and compact spectrometers, researchers have explored the possibilities of taking the advantages of metasurfaces such as its flexibility to design arbitrary phase response or convenience to be integrated to other optical system to create multifunctional meta-lens-based spectrometers [20,21,37–39]. Spectrometers based on off-axis meta-lenses was first explored by Khorasaninejad et al. [20], which unambiguously shows the potential of the technique, i.e., meta-lenses, as an alternative way to build spectrometers. However, a more detailed parametric analysis is required to fully understand the features of the two-dimensional device,

especially clarifying the performance dependencies (spectral range and spectral resolution) on the system’s structural parameters (lens aperture, focal length, off-axis angle and orientation angle of the detector plane). These information is crucial for the device design and the dispersive characteristics of off-axis meta-lenses need to be further illustrated.

In this paper, we carry out a comprehensive characteristic analysis of off-axis meta-lens based compact spectrometers using both rigorous wave theory and geometrical ray optics. The dispersive properties of the off-axis meta-lens provide the technique foundation for spectroscopy. We first show that by optimizing the orientation angle of the output (detector) plane, the effective spectral range can be enhanced about three times than that of the common configuration where the output plane is placed perpendicular to the optical axis. From the numerical diffraction calculations compared with the analytical geometrical optics analysis, we then discuss the full picture about the structural dependence of the intrinsic performance of the device. It is found that to design a high-resolution spectrometer, the aperture diameter and off-axis angle of the meta-lens should be enlarged as much as possible. On the contrary, a broadband spectrometer can be designed at certain sacrifice of spectral resolution by reducing the lens’s aperture and off-axis angle and increasing the focal length. Based on these features, we give two concrete device designs: one could cover the 800–1800 nm band with the spectral resolution of 2–5 nm and the other covering the 780–920 nm band with a finer spectral resolution of 0.15–0.6 nm. The current research provides a new perspective to design meta-lens-based spectrometers.

2. Design Principle of Spectrometer Based on Off-Axis Meta-Lens

A schematic diagram of the meta-lens-based spectrometer is shown in Figure 1. For practice, a collimation light circuit is basically required for the proposed device (not shown in Figure 1). For the off-axis meta-lens which will focus the incident normal plane wave at a deflected angle α , the phase distribution φ_d imparted by it follows

$$\varphi_d(x, y) = 2\pi - \frac{2\pi}{\lambda_d} (\sqrt{(x - f \sin \alpha)^2 + y^2 + (f \cos \alpha)^2} - f), \tag{1}$$

where λ_d is the design wavelength (corresponding to λ_2 in Figure 1) and f is the focal length.

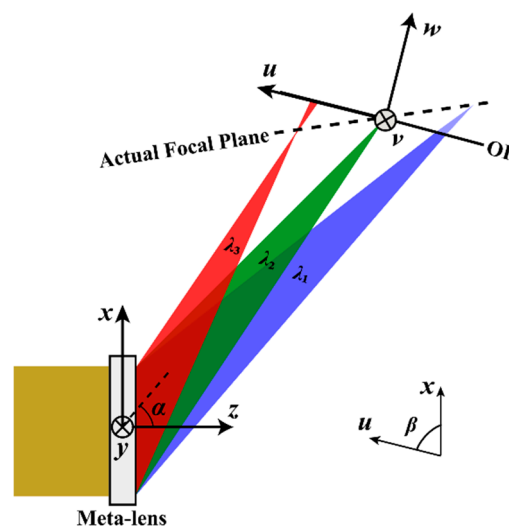


Figure 1. Schematic illustration showing the configuration of the spectrometer based on an off-axis meta-lens. The design wavelength is λ_2 and the off-axis angle is α . The actual focal plane denoted by the dashed line has a skew orientation angle with the optical axis. The angle between the u -axis and the x -axis is defined as the orientation angle of the output plane (OP) β . The inset shows the definition of its sign. In addition to the global coordinate system (x, y, z) based on the meta-lens, a local coordinate system (u, v, w) based on the OP is adopted to simplify the deduction.

Two kinds of chromatics dispersion are introduced according to this configuration—the longitudinal displacement along the optical axis (the line from the center of the meta-lens to the focal point of the design wavelength) and lateral displacement perpendicular to the optical axis [21,40]. It can be predicted that the actual focal plane for light with different wavelengths (λ_1 , λ_2 and λ_3 indicated in Figure 1 as an illustration) has a skew orientation angle with the optical axis. The output plane (OP) where the detector is placed does not always coincide with the actual focal plane in practice. A local coordinate system (u, v, w) centered at the focal point of the design wavelength ($f \sin \alpha, 0, f \cos \alpha$) is introduced at a relation with (x, y, z) by

$$\begin{cases} x = u \cos \beta + w \sin \beta + f \sin \alpha, \\ y = v, \\ z = -u \sin \beta + w \cos \beta + f \cos \alpha, \end{cases} \quad (2)$$

where β denotes the angle between the u -axis and the x -axis. At the designing wavelength, the meta-lens will work as a blazed grating. At other frequencies, diffraction will be the dominant factor to decide the output field. In practice, the meta-lenses are usually constructed using subwavelength elements that have ideally a linear dispersion so that there is a dominant diffraction order for different frequencies in the band and their refractive angles are solely decided by the local period. Therefore, in ray optics, the meta-lens could be represented by a constant and frequency-independent phase profile. This assumption is also valid for wave optics when a meta-lens of broadband response is employed, as we assumed, for example the one consisting of Pancharatnam-Berry phase elements working for circularly polarized waves [20,21]. Then, the input field $U_i(x, y, 0)$ is written as

$$U_i(x, y, 0) = P(x, y) \exp(i\varphi_d(x, y)), \quad (3)$$

where $P(x, y)$ is the pupil function of the meta-lens. It takes nonzero and unity value only inside the meta-lens aperture. Based on Rayleigh-Sommerfeld’s diffraction formula, the output field $U_o(u, v, 0)$ is expressed by [41]

$$\begin{cases} U_o(u, v, 0) = \frac{1}{i\lambda} \iint U_i(x, y, 0) \frac{\exp(i2\pi r/\lambda)}{r^2} (-u \sin \beta + f \cos \alpha) dx dy, \\ r = \sqrt{(u \cos \beta + f \sin \alpha - x)^2 + (v - y)^2 + (-u \sin \beta + f \cos \alpha)^2}, \end{cases} \quad (4)$$

where r denotes the distance from the source ($x, y, 0$) to the observation point ($u, v, 0$) (local coordinate system).

3. Results and Discussion

3.1. Simulation Results of a Typical Meta-Lens-Based Spectrometer

It is pivotal to analyze the dispersive characteristics of the spectrometer based on the off-axis meta-lens first. According to Equations (1)–(4), here we give the simulation results of the configuration with parameters $f = 20$ mm, aperture diameter $D = 2$ mm, $\alpha = 45^\circ$ and $\beta = 45^\circ$ (the OP is perpendicular to the optical axis) at $\lambda_d = 1550$ nm, as shown in Figure 2. It corresponds to a small numerical aperture $NA = 0.035$ (see Equation (5) below). The focal line profile along the u -axis as λ varies in 1520–1580 nm is shown in Figure 2a. The dispersion-caused spatial focal spot distribution ensures the technical practicability to develop a meta-lens based spectrometer. One can see the focal line gets widened obviously as wavelength significantly deviates from the design wavelength due to the chromatic aberration and the mismatch of the actual focal plane and the OP. In this spectral range, the displacement Δu is nearly linearly dependent on wavelength, suggesting a linear dispersion $du/d\lambda = 9.95 \mu\text{m}/\text{nm}$. A diffraction-limited spatial full width at half-maximum (FWHM) of the focal spot of $19.6 \mu\text{m}$ ($12.6 \lambda_d$) at $\lambda_d = 1550$ nm is observed from Figure 2b. It raises slowly as wavelength deviates from λ_d . We introduce the effective spectral range $\Delta\lambda$ to evaluate the performance of the

spectrometer. Within this spectral range, the FWHM of the spot line is less than 1.2 times $\text{FWHM}|_{\lambda=\lambda_d}$. In fact, this criterion is much stringent compared with previous studies about optical spectrometers and the commercial products [21]. For the configuration proposed here, $\Delta\lambda = 1574 \text{ nm} - 1526 \text{ nm} = 48 \text{ nm}$. The spectral resolution $\delta\lambda$ as a function of wavelength define by the FWHM value of the $U_o(\lambda)$ curve is also shown in Figure 2b. The inset of Figure 2b plots the $U_o(\lambda)$ intensity along the dashed line in Figure 2a at $u = 0$. Over the spectral range 1524–1574 nm, the spectral resolution is within 1.8 nm. Figure 2c plots the field intensity (normalized by the maximum of the field intensity at the design wavelength λ_d) profile along the u -axis at different wavelengths at an interval of 1.5 nm. Different spectral lines are distinguishable in this interval. These results are acquired without considering the actual pixel size of the detector.

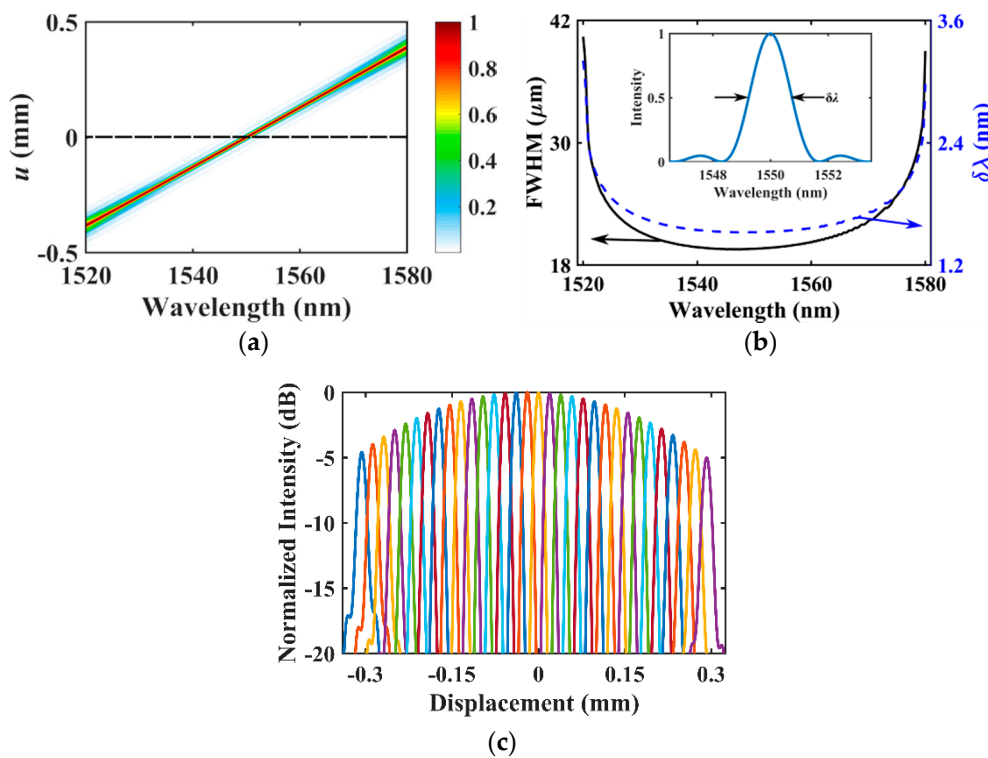


Figure 2. Dispersive characteristics of a meta-lens-based spectrometer: (a) The focal line along the u -axis as a function of wavelength for the configuration with $f = 20 \text{ mm}$, aperture diameter $D = 2 \text{ mm}$, $\alpha = 45^\circ$ and $\beta = 45^\circ$; (b) FWHM and spectral resolution $\delta\lambda$ of the focal line as a function of wavelength. Inset shows the field profile along the dashed line in (a); (c) Electric field intensity normalized by the maximum of the field intensity at the design wavelength on the OP at different wavelengths (from 1526 to 1574 nm at a constant interval of 1.5 nm).

3.2. Relationship between Structural Parameters and Evaluation Indexes of Spectrometer

As mentioned above, the disorientation of the actual focal plane with the output plane restricts the effective spectral range of the meta-lens-based spectrometer. We simulate the output field of system with different orientation angles of the OP β while other parameters are kept constant as those used in Figure 2 and analyze the effective spectral ranges $\Delta\lambda$ and spectral resolutions $\delta\lambda$ of them (shown in Figure 3a). The lower and upper bounds of the blue band in Figure 3a denote the minimum and maximum spectral resolution, respectively, which roughly have a constant ratio. The spectral range $\Delta\lambda$ reaches the maximum at about 140 nm (almost three times larger than that at $\beta = 45^\circ$ in Figure 2) when β is about -70° . According to the above discussions, it is obvious that the effective spectral range will reach maximum when the OP overlaps the actual focal plane because of the decrease of the aberration. On the other hand, when the OP is nearly perpendicular to the actual focal plane, the effective spectral

range loses its physical meaning. The spectral resolution $\delta\lambda$ is nearly independent on β and primarily decided by the structural parameters of the meta-lens (they are the aperture diameter, the focal length and the off-axis angle). Although the linear dispersion will increase when the orientation of OP is overlapped with the actual focal plane, the size of the focal spot will also increase proportionally.

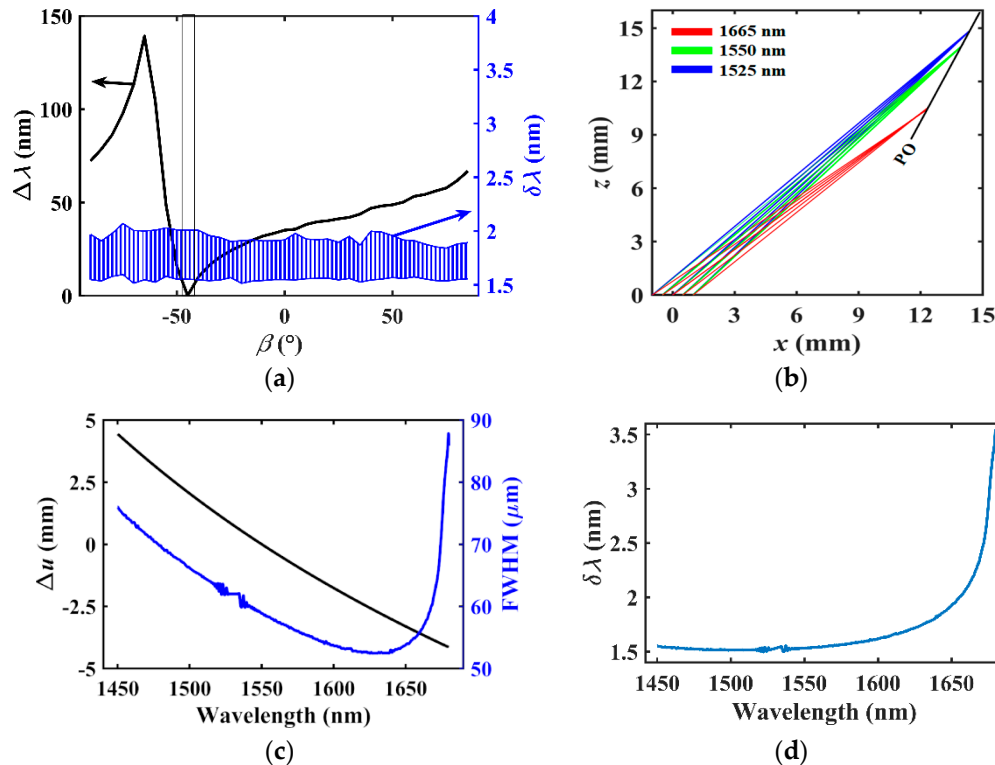


Figure 3. Influences of the orientation angle of the OP β on the dispersive properties of the meta-lens: (a) The effective spectral range $\Delta\lambda$ and spectral resolution $\delta\lambda$ as a function of β . Arrows ascribe the curves to the left or right y -axis. The data for β close to -45° (indicated by the gray box) has low accuracy because the OP is parallel to the optical axis at this specific case; (b) Ray tracing calculations for the meta-lens at wavelengths of 1525, 1550 and 1665 nm, respectively, indicating an optimal orientation angle $\beta = -70^\circ$; (c) Displacement Δu and FWHM of the focal line as a function of wavelength at $\beta = -70^\circ$; (d) Spectral resolution $\delta\lambda$ as a function of wavelength at $\beta = -70^\circ$.

Based on the above analysis, hereafter we go a step further to study the optimal value of β according to the ray tracing method. Adoption of the method is reasonable because the geometrical optics approximation is available for our low NA design. A commercial software Zemax 2005 (Zemax LLC, Kirkland, WA, USA, 2005) was used to trace the light path at three wavelengths (1525 nm, 1550 nm, 1665 nm), as shown in Figure 3b. We adopt the Zernike standard phase surface deduced from Equation (1) [42]. We choose 1525 and 1665 nm as simulation wavelengths because they are the lower and upper bounds of the effective spectral range. The ray tracing results suggest that the optimal orientation angle is $\beta = -70^\circ$, which agrees exactly with the prediction of wave analysis. The displacement Δu and FWHM of the focal line as a function of the operation wavelength at $\beta = -70^\circ$ are shown in Figure 3c. The position of the minimum FWHM of the focal line red-shifts to the wavelength 1640 nm due to the extremely oblique orientation angle relative to the optical axis. The displacement of the focal line is not linearly dependent on wavelength anymore. Figure 3d gives the spectral resolution $\delta\lambda$ as a function of wavelength at $\beta = -70^\circ$. The spectral resolution below 1.6 nm is obtained over a wide spectral range from 1450 to 1600 nm. Although the effective spectral range will be greatly enhanced by adjusting the orientation angle of the OP, the actual working efficiency of the device may degrade due to the reduced photon absorption efficiency of detector at grazing incident angles. In principle, this

problem may be overcome by patterning the detector with another metasurface. In the following, we will restrict the discussions by using the condition $\beta = \alpha$ (i.e., the OP is perpendicular to the optical axis). This will not lose the generality to illustrate the features of spectrometers that can be reproduced with different specifications.

There are three factors that affect the performance of the meta-lens-based spectrometer besides β : aperture diameter D , focal length f and off-axis angle α . For the meta-lens, NA is expressed as

$$NA = \sin\left(\frac{1}{2} \tan^{-1} \frac{4F \cos \alpha}{4F^2 - 1}\right), \tag{5}$$

where the F -number is $F = f/D$. The influences of D, f and α on $\Delta\lambda$ and $\delta\lambda$ are presented in Figure 4. Same as above, the lower and upper bounds of the blue band denote the minimum and maximum spectral resolution, respectively. According to the calculation results, the effective spectral range $\Delta\lambda$ is linearly proportional to the focal length f but the spectral resolution $\delta\lambda$ is nearly independent on f . However, $\Delta\lambda$ and $\delta\lambda$ both show an inverse relation with the aperture diameter D and the off-axis angle α . The configuration with large f or small D and α attains wider effective spectral range due to the smaller spherical aberration [43].

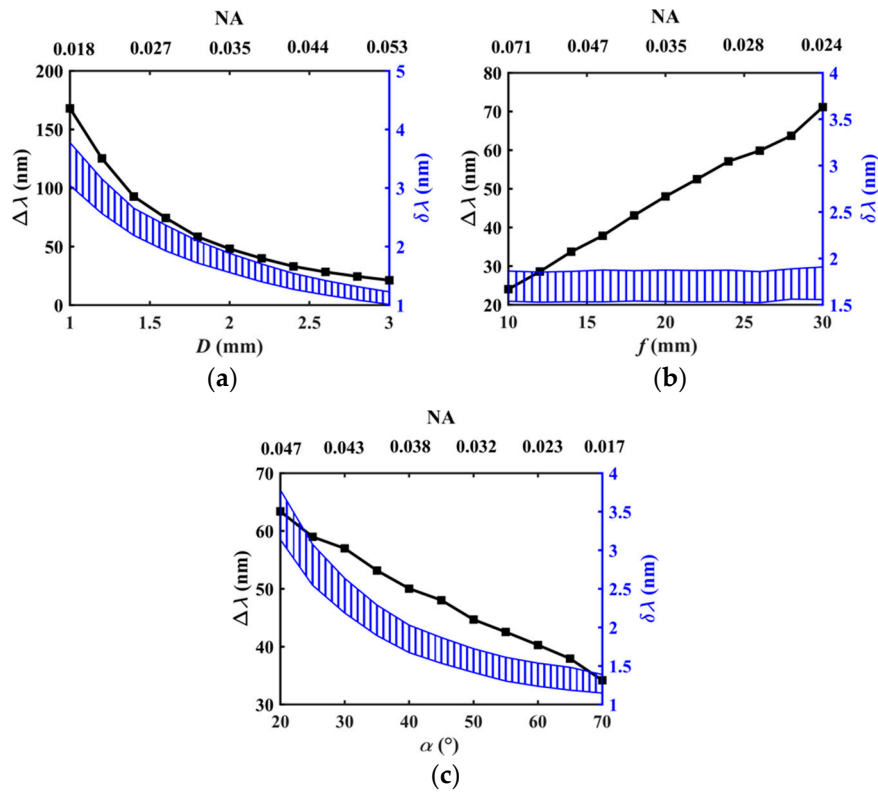


Figure 4. Effective spectral range $\Delta\lambda$ and spectral resolution $\delta\lambda$ as a function of aperture diameter D when $f = 20$ mm and $\alpha = 45^\circ$ (a); focal length f when $D = 2$ mm and $\alpha = 45^\circ$ (b); off-axis angle α when $D = 2$ mm and $f = 20$ mm.

From the wave theory and the linear dispersion $du/d\lambda$ for $\beta = \alpha$ (see Figure 2b), the spectral resolution can be estimated by [20]

$$\delta\lambda = \frac{d\lambda}{f \{ \sin^{-1} [(1 + \frac{d\lambda}{\lambda_d}) \sin \alpha] - \alpha \}} \times \frac{0.5\lambda}{NA}. \tag{6}$$

For a large F -number ($F > 6$ in our case), Equation (5) can be simplified as

$$NA \approx \frac{1}{2} \tan^{-1} \frac{4F \cos \alpha}{4F^2 - 1} \approx \frac{2F \cos \alpha}{4F^2 - 1}. \tag{7}$$

Then the spectral resolution at the design wavelength $\delta\lambda|_{\lambda=\lambda_d}$ is

$$\delta\lambda|_{\lambda=\lambda_d} = \lim_{d\lambda \rightarrow 0} \delta\lambda = \frac{0.5\lambda_d^2}{f \tan \alpha \times NA} = \frac{\lambda_d^2}{D \sin \alpha} \left[1 - \left(\frac{1}{2F} \right)^2 \right] \approx \frac{\lambda_d^2}{D \sin \alpha}. \tag{8}$$

According to Figure 2c, it is reasonable to approximate the minimum spectral resolution to be equal to $\delta\lambda|_{\lambda=\lambda_d}$ for $\beta = \alpha$. Then we conclude that the minimum spectral resolution is inversely proportional to D or the sine of α and nearly independent of f for meta-lens with a large F -number. The analytical result according to Equation (8) provides almost the same variation tendency with the numerical results.

3.3. Two Practical Device for Different Applications

Consider the fact that the detector always has limited element sizes and array numbers, there will be a trade-off between the effective spectral range and spectral resolution in designing spectrometer. A high-resolution spectrometer with a wide spectral range is ideal but not realistic for the grating based species. Alternatively, we propose two practical configurations to satisfy the actual requirements: a wideband spectrometer with medium spectral resolution and a narrowband spectrometer with high spectral resolution. In practice, the meta-lens based approach has the advantages to integrate these two or more components into a single package.

The structural parameters for the wideband spectrometer with medium spectral resolution are $f = 30$ mm, $D = 2$ mm, $\alpha = 15^\circ$, $\beta = -89^\circ$ at $\lambda_d = 1550$ nm. Its focal line along the u -axis and spectral resolution as a function of wavelength are shown in Figure 5a,b, respectively, indicating a remarkably wide spectral range. This device will work at the band 800–1800 nm with the spectral resolution of 2–5 nm. The dimension of this configuration is estimated as $70 \times 20 \times 10$ mm³. This configuration is compact and its spectral range and spectral resolution is comparable to the traditional commercial mini-spectrometer that has the similar working parameters, for example, Hamamatsu Photonics C11482GA [44]. The structural parameters for the narrowband spectrometer with high spectral resolution are $f = 30$ mm, $D = 6$ mm, $\alpha = 45^\circ$, $\beta = -65^\circ$ at $\lambda_d = 850$ nm. Its focal line along the u -axis and the spectral resolution as a function of wavelength are shown in Figure 5b,c, respectively, indicating a narrow spectral range 780–920 nm. Within this spectral range, the spectral resolution is within 0.15–0.6 nm. Its dimension is approximately $40 \times 30 \times 10$ mm³. This results are also comparable to the traditional commercial spectrometer such as Hamamatsu Photonics C13054MA [44].

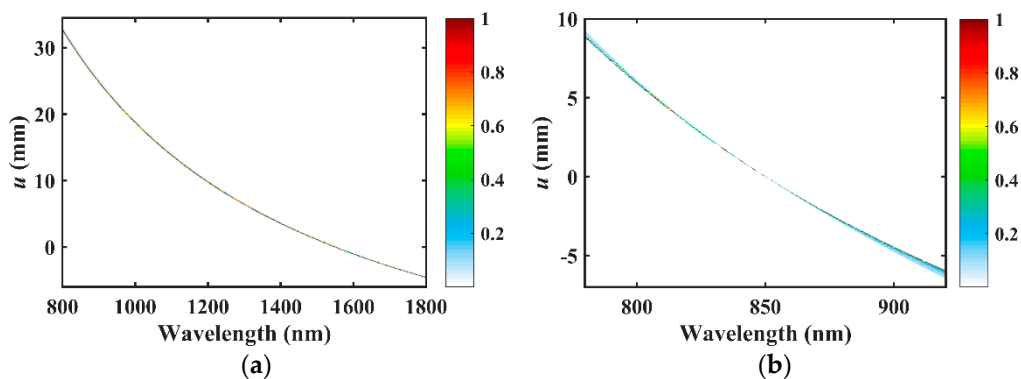


Figure 5. Cont.

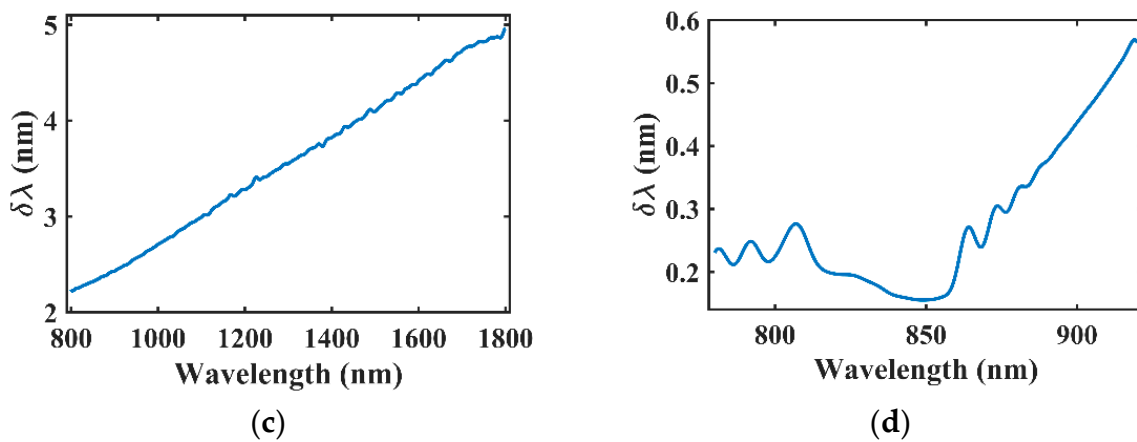


Figure 5. Two practical configurations for the actual application prospects: (a) The focal line along the u -axis as a function of wavelength for the configuration with $f = 30$ mm, $D = 2$ mm, $\alpha = 15^\circ$ and $\beta = -89^\circ$ at $\lambda_d = 1550$ nm; (b) The focal line along the u -axis as a function of wavelength for the configuration with $f = 30$ mm, $D = 6$ mm, $\alpha = 45^\circ$ and $\beta = -65^\circ$ at $\lambda_d = 850$ nm; (c) Spectral resolution $\delta\lambda$ as a function of wavelength of the configuration in (a); (d) Spectral resolution $\delta\lambda$ as a function of wavelength of the configuration in (b).

In practice, one can determine the initial parameters of the meta-lens according to Equation (8) to meet the requirements of the spectral resolution. The effective spectral range could be broadened obviously by adjusting the orientation angle of the OP β according to the ray tracing method. These parameters together give the freedoms to design spectrometer for various application requirements.

3.4. Influence of the Fabrication Error Analysis

In this section, we give a numerical analysis how the imperfect implementation may affect the performance of the proposed device. To do so, we have assumed that any imperfection in fabrication may cause the phase distortion of the ideal device from Equation (1).

Figure 6a gives the effective spectral range $\Delta\lambda$, the spectral resolution $\delta\lambda$ and the maximum intensity I_m of the focal spot. The latter two are taken at the design wavelength. In the calculation, a random noise using the built-in function of the MATLAB is applied to the phase profile in Equation (1), whose value obeys a normal distribution $\mathcal{N}(0, \sigma^2)$. Here, σ denotes the standard deviation. It is seen that the maximum intensity I_m decreases when the value σ increases, indicating the weakened focusing efficiency at larger phase distortion. However, the effective spectral range and the spectral resolution at the design wavelength almost remain stable as σ changes because they are solely contributed by the zeroth diffraction order. These effects could be more clearly understood from the focusing pattern plotted in Figure 6b–d at $\sigma = 0^\circ$, 90° and 120° , respectively. The spatial characteristics of the zeroth diffraction order are hardly influenced when the phase distortion gets more deteriorated. Its intensity decreases as the unwanted higher diffraction orders become stronger. For practice, we can expect that the proposed off-axis meta-lens can suffer a spatial phase distortion with the largest deviation less than 48° corresponding to a 50% amplitude reduction where the higher diffraction orders are thought weakly enough and have no influence on the performance of the spectrometer. This is relatively a large tolerance and allows the device to be precisely implemented.

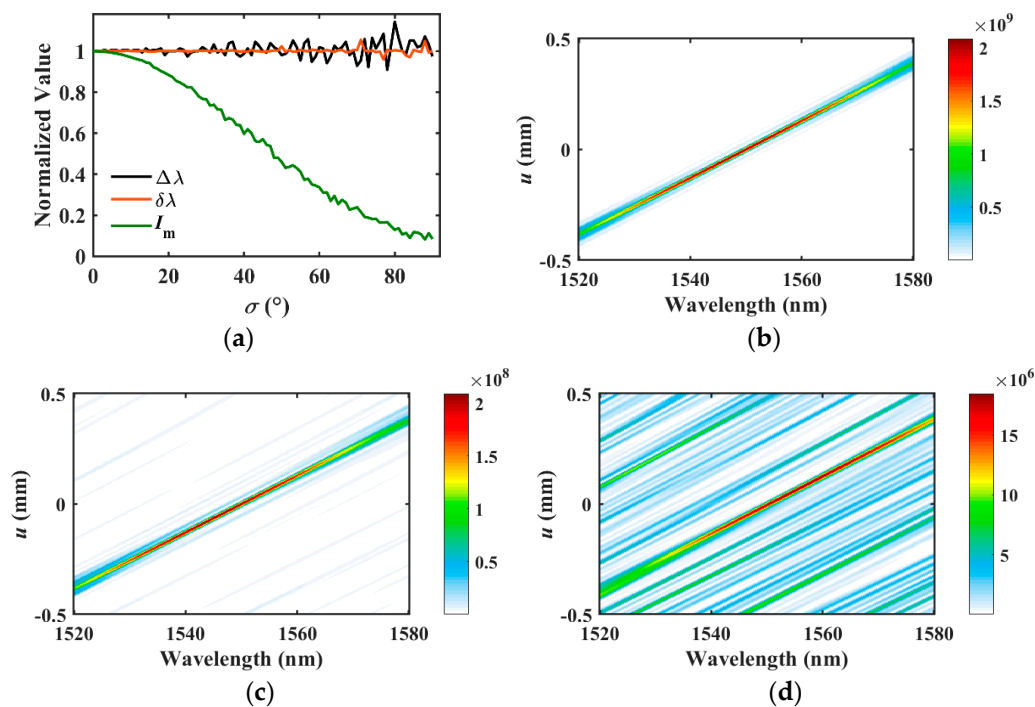


Figure 6. Influence of error analysis: (a) The effective spectral range $\Delta\lambda$ (black), the spectral resolution $\delta\lambda$ (red) and the maximum intensity I_m (green) of focal spot changing as a function of the random phase error factor σ . The values are normalized by those at $\sigma = 0$. Here the added spatial phase distortion value obeys a normal distribution $\mathcal{N}(0, \sigma^2)$ realized by the built-in random function in MATLAB; (b–d) The focus pattern of the proposed off-axis meta-lens at $\sigma = 0^\circ, 90^\circ$ and 120° , respectively.

4. Conclusions

In this paper, the relationship between the performance of the off-axis meta-lens-based spectrometer and the structural parameters of the system are studied theoretically. It is shown that the desired effective spectral range $\Delta\lambda$ and the spectral resolution $\delta\lambda$ can be realized by properly selecting the designing parameters of focal length f , aperture diameter D , off-axis angle α and orientation angle of output plane β . Based on these, we designed two device configurations able to work for (i) broadband spectroscopy in 800–1800 nm with the low spectral resolution of 2–5 nm and (ii) narrowband spectroscopy in 780–920 nm with the high spectral resolution of 0.15–0.6 nm. These results will be helpful to guiding the design of compact spectrometer with specific response characteristics for various applications.

Acknowledgments: The authors are grateful to the partial supports from NSFC of Zhejiang Province (LR15F050001& LZ17A040001), NSFC (61775195) and the National Key Research and Development Program of China (No. 2017YFA0205700).

Author Contributions: Yi Zhou performed the simulations, analyzed the data and wrote the paper; Rui Chen provided the main instructions of the simulation methods; Yungui Ma supervised this study and revised the paper.

Conflicts of Interest: The authors declare no conflict of interest.

References

1. Staude, I.; Schilling, J. Metamaterial-Inspired Silicon Nanophotonics. *Nat. Photonics* **2017**, *11*, 274–284. [[CrossRef](#)]
2. Liu, L.; Zhang, X.; Kenney, M.; Su, X.; Xu, N.; Ouyang, C.; Shi, Y.; Han, J.; Zhang, W.; Zhang, S. Broadband Metasurfaces with Simultaneous Control of Phase and Amplitude. *Adv. Mater.* **2014**, *26*, 5031–5036. [[CrossRef](#)] [[PubMed](#)]

3. Ni, X.; Emani, N.K.; Kildishev, A.V.; Boltasseva, A.; Shalae, V.M. Broadband Light Bending with Plasmonic Nanoantennas. *Science* **2012**, *335*, 427. [[CrossRef](#)] [[PubMed](#)]
4. Pors, A.; Nielsen, M.G.; Eriksen, R.L.; Bozhevolnyi, S.I. Broadband Focusing Flat Mirrors Based on Plasmonic Gradient Metasurfaces. *Nano Lett.* **2013**, *13*, 829–834. [[CrossRef](#)] [[PubMed](#)]
5. Arbabi, A.; Horie, Y.; Bagheri, M.; Faraon, A. Dielectric Metasurfaces for Complete Control of Phase and Polarization with Subwavelength Spatial Resolution and High Transmission. *Nat. Nanotechnol.* **2015**, *10*, 937–943. [[CrossRef](#)] [[PubMed](#)]
6. Balthasar Mueller, J.P.; Rubin, N.A.; Devlin, R.C.; Groever, B.; Capasso, F. Metasurface Polarization Optics: Independent Phase Control of Arbitrary Orthogonal States of Polarization. *Phys. Rev. Lett.* **2017**, *118*, 113901. [[CrossRef](#)] [[PubMed](#)]
7. Khorasaninejad, M.; Crozier, K.B. Silicon Nanofin Grating as a Miniature Chirality-Distinguishing Beam-Splitter. *Nat. Commun.* **2014**, *5*, 5386. [[CrossRef](#)] [[PubMed](#)]
8. Arbabi, A.; Arbabi, E.; Kamali, S.M.; Horie, Y.; Han, S.; Faraon, A. Miniature Optical Planar Camera Based on a Wide-Angle Metasurface Doublet Corrected for Monochromatic Aberrations. *Nat. Commun.* **2016**, *7*, 13682. [[CrossRef](#)] [[PubMed](#)]
9. Wen, D.; Yue, F.; Ardron, M.; Chen, X. Multifunctional Metasurface Lens for Imaging and Fourier Transform. *Sci. Rep.* **2016**, *6*, 27628. [[CrossRef](#)] [[PubMed](#)]
10. Yang, H.; Li, G.; Su, X.; Cao, G.; Zhao, Z.; Chen, X.; Lu, W. Reflective Metalens with Sub-Diffraction-Limited and Multifunctional Focusing. *Sci. Rep.* **2017**, *7*, 12632. [[CrossRef](#)] [[PubMed](#)]
11. Khorasaninejad, M.; Zhu, A.Y.; Roques-Carnes, C.; Chen, W.T.; Oh, J.; Mishra, I.; Devlin, R.C.; Capasso, F. Polarization-Insensitive Metalenses at Visible Wavelengths. *Nano Lett.* **2016**, *16*, 7229–7234. [[CrossRef](#)] [[PubMed](#)]
12. Khorasaninejad, M.; Chen, W.T.; Zhu, A.Y.; Oh, J.; Devlin, R.C.; Rousso, D.; Capasso, F. Multispectral Chiral Imaging with a Metalens. *Nano Lett.* **2016**, *16*, 4595–6000. [[CrossRef](#)] [[PubMed](#)]
13. Chen, W.T.; Zhu, A.Y.; Khorasaninejad, M.; Shi, Z.; Sanjeev, V.; Capasso, F. Immersion Meta-Lenses at Visible Wavelengths for Nanoscale Imaging. *Nano Lett.* **2017**, *17*, 3188–3194. [[CrossRef](#)] [[PubMed](#)]
14. Groever, B.; Chen, W.T.; Capasso, F. Meta-Lens Doublet in the Visible Region. *Nano Lett.* **2017**, *17*, 4902–4907. [[CrossRef](#)] [[PubMed](#)]
15. Ni, X.; Kildishev, A.V.; Shalae, V.M. Metasurface Holograms for Visible Light. *Nat. Commun.* **2013**, *4*, 2807. [[CrossRef](#)]
16. Chen, W.T.; Yang, K.Y.; Wang, C.M.; Huang, Y.W.; Sun, G.; Chiang, I.D.; Liao, C.Y.; Hsu, W.L.; Lin, H.T.; Sun, S.; et al. High-Efficiency Broadband Meta-Hologram with Polarization-Controlled Dual Images. *Nano Lett.* **2014**, *14*, 225–230. [[CrossRef](#)] [[PubMed](#)]
17. Wen, D.; Yue, F.; Li, G.; Zheng, G.; Chan, K.; Chen, S.; Chen, M.; Li, K.F.; Wong, P.W.H.; Cheah, K.W.; et al. Helicity Multiplexed Broadband Metasurface Holograms. *Nat. Commun.* **2015**, *6*, 8241. [[CrossRef](#)] [[PubMed](#)]
18. Zheng, G.; Mühlenbernd, H.; Kenney, M.; Li, G.; Zentgraf, T.; Zhang, S. Metasurface Holograms Reaching 80% Efficiency. *Nat. Nanotechnol.* **2015**, *10*, 308–312. [[CrossRef](#)] [[PubMed](#)]
19. Zhang, C.; Yue, F.; Wen, D.; Chen, M.; Zhang, Z.; Wang, W.; Chen, X. Multichannel Metasurface for Simultaneous Control of Holograms and Twisted Light Beams. *ACS Photonics* **2017**, *4*, 1906–1912. [[CrossRef](#)]
20. Khorasaninejad, M.; Chen, W.T.; Oh, J.; Capasso, F. Super-Dispersive Off-Axis Meta-Lenses for Compact High Resolution Spectroscopy. *Nano Lett.* **2016**, *16*, 3732–3737. [[CrossRef](#)] [[PubMed](#)]
21. Zhu, A.Y.; Chen, W.T.; Khorasaninejad, M.; Oh, J.; Zaidi, A.; Mishra, I.; Devlin, R.C.; Capasso, F. Ultra-Compact Visible Chiral Spectrometer with Meta-Lenses. *APL Photonics* **2017**, *2*, 036103. [[CrossRef](#)]
22. Minovich, A.E.; Miroshnichenko, A.E.; Bykov, A.Y.; Murzina, T.V.; Neshev, D.N.; Kivshar, Y.S. Functional and Nonlinear Optical Metasurfaces. *Laser Photonics Rev.* **2015**, *9*, 195–213. [[CrossRef](#)]
23. Walter, F.; Li, G.; Meier, C.; Zhang, S.; Zentgraf, T. Ultrathin Nonlinear Metasurface for Optical Image Encoding. *Nano Lett.* **2017**, *17*, 3171–3175. [[CrossRef](#)] [[PubMed](#)]
24. Zhang, L.; Mei, Z.L.; Zhang, M.R.; Yang, F.; Cui, T.J. An Ultrathin Directional Carpet Cloak Based on Generalized Snell's Law. *Appl. Phys. Lett.* **2013**, *103*, 151115. [[CrossRef](#)]
25. Ni, X.; Wong, Z.J.; Mrejen, M.; Wang, Y.; Zhang, X. An Ultrathin Invisibility Skin Cloak for Visible Light. *Science* **2015**, *349*, 1310–1314. [[CrossRef](#)] [[PubMed](#)]

26. Yang, Y.; Jing, L.; Zheng, B.; Hao, R.; Yin, W.; Li, E.; Soukoulis, C.M.; Chen, H. Full-Polarization 3D Metasurface Cloak with Preserved Amplitude and Phase. *Adv. Mater.* **2016**, *28*, 6866–6871. [[CrossRef](#)] [[PubMed](#)]
27. Born, M.; Wolf, E. *Principles of Optics: Electromagnetic Theory of Propagation, Interference and Diffraction of Light*, 7th ed.; Cambridge University Press: Cambridge, UK, 1999, ISBN 978-0-521-64222-4.
28. Bao, J.; Bawendi, M.G. A Colloidal Quantum Dot Spectrometer. *Nature* **2015**, *523*, 67–70. [[CrossRef](#)] [[PubMed](#)]
29. Henstridge, M.; Zhou, J.; Guo, L.J.; Merlin, R. Wavelength Scale Terahertz Spectrometer Based on Extraordinary Transmission. *Appl. Phys. Lett.* **2017**, *111*, 063503. [[CrossRef](#)]
30. Yuan, L.; He, Z.; Lv, G.; Wang, Y.; Li, C.; Xie, J.; Wang, J. Optical Design, Laboratory Test, and Calibration of Airborne Long Wave Infrared Imaging Spectrometer. *Opt. Express* **2017**, *25*, 22440–22454. [[CrossRef](#)] [[PubMed](#)]
31. Cook, T. Anamorphic Integral Field Spectrometer for Diffuse Ultraviolet Astronomy. *Appl. Opt.* **2013**, *52*, 8765–8770. [[CrossRef](#)] [[PubMed](#)]
32. Cataldo, G.; Hsieh, W.-T.; Huang, W.-C.; Moseley, S.H.; Stevenson, T.R.; Wollack, E.J. Micro-Spec: An Ultracompact, High-Sensitivity Spectrometer for Far-Infrared and Submillimeter Astronomy. *Appl. Opt.* **2014**, *53*, 1094–1102. [[CrossRef](#)] [[PubMed](#)]
33. Zavvari, A.; Islam, M.T.; Anwar, R.; Abidin, Z.Z.; Asillam, M.F.; Monstein, C. Analysis of Radio Astronomy Bands Using CALLISTO Spectrometer at Malaysia-UKM Station. *Exp. Astron.* **2016**, *41*, 185–195. [[CrossRef](#)]
34. Udeigwe, T.K.; Young, J.; Kandakji, T.; Weindorf, D.C.; Mahmoud, M.A.; Stietiya, M.H. Elemental Quantification, Chemistry, and Source Apportionment in Golf Course Facilities in a Semi-Arid Urban Landscape Using a Portable X-Ray Fluorescence Spectrometer. *Solid Earth* **2015**, *6*, 415–424. [[CrossRef](#)]
35. Buzan, E.M.; Beale, C.A.; Boone, C.D.; Bernath, P.F. Global Stratospheric Measurements of the Isotopologues of Methane from the Atmospheric Chemistry Experiment Fourier Transform Spectrometer. *Atmos. Meas. Tech.* **2016**, *9*, 1095–1111. [[CrossRef](#)]
36. Mantouvalou, I.; Lachmann, T.; Singh, S.P.; Vogel-Mikuš, K.; Kanngießler, B. Advanced Absorption Correction for 3D Elemental Images Applied to the Analysis of Pearl Millet Seeds Obtained with a Laboratory Confocal Micro X-ray Fluorescence Spectrometer. *Anal. Chem.* **2017**, *89*, 5453–5460. [[CrossRef](#)] [[PubMed](#)]
37. Shaltout, A.; Liu, J.; Kildishev, A.; Shalaev, V. Photonic Spin Hall Effect in Gap Plasmon Metasurfaces for On-Chip Chiroptical Spectroscopy. *Optica* **2015**, *2*, 860–863. [[CrossRef](#)]
38. Maguid, E.; Yulevich, I.; Veksler, D.; Kleiner, V.; Brongersma, M.L.; Hasman, E. Photonic Spin-Controlled Multifunctional Shared-Aperture Antenna Array. *Science* **2016**, *352*, 1202–1206. [[CrossRef](#)] [[PubMed](#)]
39. Ding, F.; Pors, A.; Chen, Y.; Zenin, V.A.; Bozhevolnyi, S.I. Beam-Size-Invariant Spectropolarimeters Using Gap-Plasmon Metasurfaces. *ACS Photonics* **2017**, *4*, 943–949. [[CrossRef](#)]
40. Zhou, Y.; Chen, R.; Ma, Y. Design of Optical Wavelength Demultiplexer Based on Off-Axis Meta-Lens. *Opt. Lett.* **2017**, *42*, 4716–4719. [[CrossRef](#)] [[PubMed](#)]
41. Goodman, J.W. *Introduction to Fourier Optics*, 3rd ed.; Roberts & Company Publishers: Englewood, IL, USA, 2005, ISBN 978-0-9747077-2-3.
42. Noll, R.J. Zernike Polynomials and Atmospheric Turbulence. *J. Opt. Soc. Am. A* **1976**, *66*, 201–211. [[CrossRef](#)]
43. Welford, W.T. *Aberrations of Optical Systems*, 1st ed.; IOP Publishing: Bristol, UK, 1986, ISBN 978-0-85274-564-9.
44. Hamamatsu Mini-Spectrometers Product Page. Available online: <http://www.hamamatsu.com/eu/en/product/category/5001/4016/index.html> (accessed on 29 November 2017).

